NASA TECHNICAL MEMORANDUM 102702

DAMAGE TOLERANCE OF WOVEN GRAPHITE/EPOXY BUFFER STRIP PANELS

John M. Kennedy

August 1990

National Aeronautics and
Space Administration

Langley Research Center
Hampton, Virginia 23665-5225

ABSTRACT

Graphite/epoxy panels with S-glass buffer strips were tested in tension and shear to measure their residual strengths with crack-like damage. The buffer strips were regularly spaced narrow strips of continuous S-glass. Panels were made with a uniweave graphite cloth where the S-glass buffer material was woven directly into the cloth. Panels were made with different width and thickness buffer strips. The panels were loaded to failure while remote strain, strain at the end of the slit, and crack opening displacement were monitored. The notched region and nearby buffer strips were radiographed periodically to reveal crack growth and damage.

Except for panels with short slits, the buffer strips arrested the propagating crack. The strength (or failing strain) of the panels was significantly higher than the strength of all-graphite panels with the same length slit. Panels with wide, thick buffer strips were stronger than panels with thin, narrow buffer strips . A shear-lag model predicted the failing strength of tension panels with wide buffer strips accurately, but over-estimated the strength of the shear panels and the tension panels with narrow buffer strips.

INTRODUCTION

Advanced composites are very attractive materials for use in aircraft structures because of their high specific strengths and moduli. Unfortunately, the common graphite/epoxy systems behave in a brittle fashion; and thus, panels with damage (holes or cracks) have much lower strengths than undamaged panels. Hybrid composites (composite laminates with two or more fiber types) and buffer strip panels (panels with discrete regions of hybrid composite) have higher damage tolerance characteristics than all-graphite system ([1] and [2]) because of the mix of high and low strain fibers. Unfortunately, the hybrids are usually heavier than the all-graphite system, and the stiffness may be much lower than the all-graphite laminate. Figure 1 shows the specific moduli and specific strengths for a quasi-isotropic all-graphite panel, an S-glass/graphite hybrid laminate, and a graphite buffer strip panel with 13 mm wide S-glass buffer strips. The specific strengths shown are for 254 mm wide panels with 51 mm slits. The data are taken from [1] and [2]. The figure shows that the buffer strip panels have both the light weight and high modulus of the all-graphite composite and even better damage tolerance characteristics than the hybrid composite.

Buffer strip panels are made by replacing narrow strips of graphite plies with plies of another material such as S-glass or Kevler-49[1]. Figure 2 shows a cross-section of a typical buffer strip and panel. The strips are spaced across the width of the panel. Because the cross-sectional area of the buffer strips is small, the weight and stiffness of the panel are not appreciably affected by the dense, low modulus buffer material. The damage tolerance of the panel is improved because cracks propagating from damage are arrested by the buffer strips and the panel carries additional load before failing. The cracks are arrested because the modulus of resilience or toughness of the S-glass and Kevlar fibers is greater than that

1 Kevlar-49, Registered trademark of E. I. du Pont de Nemours and Co., Inc.

of the graphite fibers [1]. Usually delaminations and matrix cracks develop in the buffer strips ahead of the arrested cracks which elevates the residual strength even more [3].

The buffer strip panels reported in [1] were made using prepreg tape. The manufacturing cost was high because each strip of buffer material had to be individually placed into the laminate. The results reported in this paper are for panels made using a unidirectional weave cloth [4]. These panels were much cheaper to manufacture because the buffer material was incorporated into the cloth using a textile weaving process; thus, no additional labor was required to make the panel.

The objective of this paper is to compare the strengths of panels made out of uniweave cloth to those of panels made from prepreg tape. Also, several panel configurations were investigated which were not investigated in [1], and a few panels were tested in shear. Panel strengths are compared to predictions from a shear lag analysis [1].

NOMENCLATURE

a	half-length of crack, m
COD	crack-opening displacement, m
E	Young's modulus, Pa
E_o,E_b	Young's modulus of 0° Gr/Ep and 0° buffer material, respectively, Pa
G	shear modulus, Pa
h_o,h_b	thickness of a ply in basic laminate and thickness of buffer material in uniweave cloth respectively, m
K_t	strain concentration factor
K_ε	strain intensity factor, $\sqrt{m}$
$K_{\varepsilon q}$	critical strain intensity factor, $\sqrt{m}$
L_s	length of a side of the shear panels, m
Q_c	general fracture toughness parameter, $\sqrt{m}$
t	total thickness of laminate, m
W	width of tension panel
W_a	length of arrested crack or distance between buffer strips, m
W_b	width of buffer strip, m
S_c	critical failing stress, Pa
ε	axial strain
ε_{tub}	ultimate tensile strain of buffer material
ε_{tuf}	ultimate tensile strain of 0° graphite ply
ε_y^F	critical far-field tensile strain in tension panel
ε_y^P	tensile strain in infinite sheet due to compressive loading
ε_y^*	critical far-field tensile strain in shear panel
δ_c	critical damage size, m
γ	shear strain
ν	Poisson's ratio

ρ density, $\frac{kg}{m^3}$

$\tau^*_{x'y'}$ critical far-field shear stress, Pa

Subscripts

x, y, x', y' Cartesian coordinates

1,2 coordinates parallel and perpendicular to fibers

EXPERIMENTAL PROCEDURES

Materials and Specimens

The specimens were made with T300[2] graphite and S-1014[3] glass uniweave cloth. Details of the cloth, test specimens, and curing procedures are given in [4]. Figure 3 shows a sample of the cloth with the S-glass woven periodically into the cloth to form the buffer strips. The cloth had 95 percent of the fibers in the warp direction and 5 percent in the fill direction. The fill fibers were also S-glass. Three buffer strip configurations were woven into the cloth. The first configuration had one layer of S-glass fibers $\left(\frac{h_b}{h_o} = 1\right)$ with various widths; the second had two layers of S-glass (see fig. 2, $\frac{h_b}{h_o} = 2$) which were 6.4 mm wide; and the third had four layers of S-glass $\left(\frac{h_b}{h_o} = 4\right)$ which were 3.2 mm wide. Thus, some buffer strips had the same cross-sectional area of S-glass, but different widths and thicknesses. The spacing from centerline to centerline of the buffer strips was 64 mm in all cases.

Tension and shear panels were manufactured using the uniweave cloth. Figure 4 shows sketches of typical tension and shear panels and Table 1 lists laminates, buffer strip geometry, and the plies containing buffer material. All of the tension panels were 250 mm wide and 500 mm long. The shear panels were square panels 305 mm on a side. The tension panels had a quasi-isotropic lay-up and most had buffer material that was in only the 0° plies. One group of tension panels had buffer strips in all plies. All panels were 16 plies thick except one group of tension panels which was 48 plies thick. The shear panels were quasi-isotropic and cross-plied. All of the shear panels had buffer material in the 0° and 90°

2 T300: Registered Trademark of Union Carbide

3 S-1014: Registered Trademark of 3M

plies. Table 1 shows the number of panels tested for each configuration. Slits between 5 mm and 44 mm long were machined into the center of each specimen to simulate damage.

A sheet, made with the all-graphite cloth with the stacking sequence $[45/0/-45/90]_{2S}$, was cut into tensile and fracture coupons. The layout of the sheet is shown in [4]. Elastic properties and tensile strengths were determined from tests on the coupons. The fracture properties were determined from coupons which had central slits between 8 mm and 51 mm long. For reference, average properties from these tests are given in Table 2.

Test Procedures and Equipment

Both tension and shear panels were loaded to failure at about 500 N/sec in a servo-controlled, closed-loop testing machine. Load, strain, and crack-opening displacement (COD) of the slit were recorded using a digital data acquisition system. Periodically during the tests the loading was stopped, and the region around the slit was radiographed to reveal damage at the ends of the slit. An X-ray opaque dye, zinc iodide, was used to enhance the image of the damaged areas.

The shear panels were tested in a picture frame shear fixture designed to minimize the stress concentrations at the corners of the specimen [5]. The shear panels, which were 16 plies thick, were thin and could buckle before the slit could initiate fracture. Thus aluminum guide plates were used to constrain the panel from buckling. Two types of plates were used: the first covered the entire panel and the second had a central opening large enough to uncover the area around the slit and the two adjacent buffer strips. The opening facilitated radiographic examination while under load.

RESULTS AND DISCUSSION

The results of all tests are presented in Table 1 in terms of strain instead of stress so that data can readily be compared for different laminates and test types. The stress-strain response of all the specimens was linear elastic, so stress can be calculated by multiplying strains times the elastic modulus reported in Table 1.

Tension Panels

Figure 5 shows results which illustrate the basic behavior of the buffer strip panels. The fracture analysis curve is for the all-graphite laminate with no buffer strips, and it comes from a fracture analysis for composites developed by Poe [6] (see Appendix). The net strain curve is an upper limit for failure representing notch insensitive behavior of the laminate, i.e.

$$\varepsilon_y{}^F = \left(1 - \frac{2a}{W}\right)\varepsilon_{tuf}. \qquad (1)$$

The analysis by Poe is based on linear elastic fracture mechanics and includes the effects of laminate configuration and fiber ultimate strain. Typically, the correlation between the fracture analysis and experimental results from center-notched fracture coupons is excellent for all laminates that do not develop large amounts of non-critical matrix damage at the crack-tips. Failing strains for laminates that exhibit large amounts of damage at the crack-tips are greater than the prediction because the damage acts to relieve the stress concentrations in the fibers [3]. Figure 5 shows that the fracture analysis accurately predicted the strain at which the cracks propagated in the buffer strip panels. Similar data in [1] and [2] for buffer strip panels and fracture coupons all fell on or above the prediction.

Figure 5 shows the fracture was not arrested by the buffer strips in the panel with the 13 mm slit, and the panel failed at the fracture initiation strain. The buffer strips arrested the propagating crack in the panels with 25 mm and 44 mm slits. The panels with arrested cracks were then able to bear additional load, and both failed at nearly the same far-field

strain. Figure 6 shows radiographs of the panel with the 25 mm slit. The radiographs show the region around the slit and the two adjacent buffer strips; the hour-glass-shaped object in the center of the picture is the COD gage and fixture for the COD gage. The radiographs were made just before fracture initiation and just after fracture arrest. The second radiograph clearly shows the crack extending into the buffer strips with substantial delamination in the buffer strip at the end of the crack. Fracture and arrest was also indicated by a sudden increase in COD and strain in the buffer strips.

Typically, the buffer strips will arrest cracks that propagate at strains below the remote failing strain of a panel with an arrested crack. There is a small dynamic effect that may prevent crack arrest when the strain is just below the failing strain of a panel with an arrested crack. This is probably the reason the crack did not arrest in the panel with the 13 mm slit (fig. 5) even though the strain was about 8 percent below the failing strain of the panels with arrested cracks.

Figure 7 shows the average remote failing strain for all the various tension buffer strip panels with arrested cracks. Also shown is the remote failing strain for an all-graphite panel with no buffer strips and for buffer strip panels made with prepreg tape [1]. First, the figure shows that the failing strain of buffer strip panels with arrested cracks was much higher than the failing strain of an all-graphite panel with a slit the same length as the buffer strip spacing (top bar). Second, the figure shows that buffer strip panels made from uniweave cloth failed at about the same strain as panels made with prepreg tape. And third, the figure shows that varying the buffer strip width and thickness significantly changed the failing strain of the panels. Considering only the results for panels with buffer material in the 0° plies, the results show that increasing the width of the buffer strip while holding the thickness constant increased the failing strain. Considering groups of panels with the same width buffer strips, the panels with $\frac{h_b}{h_o} = 2$ or 4 had higher failing strains than panels with

$\frac{h_b}{h_o} = 1$. The dominant parameter, however, was buffer strip width because the failing strain of panels with the thickest buffer strips was less than that of panels with the widest (12.7 mm) buffer strips. Finally, the panels with buffer material in every ply failed at the highest strain. In fact, the panels failed when the strain in the net section (section taken parallel to and through the crack) reached the ultimate failing strain of a 0° graphite ply.

Figure 8 shows remote strain versus crack length data for the panels with buffer material in every ply. The panel with the 5 mm slit failed with no arrest at the same strain as the two panels which arrested. Interestingly, the strains at which the fractures initiated in the three panels are much higher than those predicted by the fracture analysis. For the panels with buffer material only in the 0° plies (fig. 5), fractures initiated at strains about equal to those predicted by the analysis. This suggests that the additional buffer strips changed the stress state around the slits. Figure 9 shows radiographs of a panel with buffer strips in every ply. The radiograph taken before initiation shows a large area of delamination extending from the ends of the slit. The radiograph taken after arrest shows an even larger delamination area extending into the buffer strips. The delaminations in this panel are much larger than in the panels with buffer material in only the 0° plies (fig. 6). References 2 and 7 showed that delamination increased the fracture strength of composite laminates by reducing the stress concentration in the fibers near the end of the slit. Thus, the higher strains should be expected for fracture initiation in the panels with buffer strips in every ply due to the large delaminations seen in the radiographs.

Remote strain plotted versus crack length is shown in figure 10 for the 48 ply tension panels with 12.7 mm wide buffer strips. Also shown for comparison are data from the 16 ply panel with 12.7 mm wide buffer strips. The figure shows that the fracture initiation strains and failing strains of the 48 ply panels were slightly lower than those of the 16 ply panels. Also the fracture initiation strains for all the panels were very close to the strain

predicted by the fracture analysis. A study of thick laminates [8] showed that fracture strains of thick laminates were smaller than those of thin laminates because the delaminations and axial splits at the end of the slit in a thick laminate were small and confined to the plies near the surfaces.

Analysis

A shear-lag model was developed in [1] to predict the strength of buffer strip panels. The model accounted for the effects of buffer strip spacing, thickness, width, and material, as well as axial splits in the buffer strip, and constraint plies (plies other than the 0° plies). The analysis assumed panel failure when the first fiber in the buffer strip next to the crack fails.

Figure 11 shows values of $\frac{\varepsilon_y{}^F}{\varepsilon_{tub}}$ from the shear-lag model and from tests, where the crack arrested, plotted against buffer strip spacing multiplied times a stiffness parameter. Test results are only shown for panels where cracks were arrested. The solid symbols are data from panels made with tape [1]. The buffer materials were S-glass, Kevlar-49, and graphite with Mylar[4]. The open symbols are data from panels made with uniweave cloth. The prediction from the model was obtained by choosing the shear-lag parameters so that the analysis correlated with the data from [1]. The analysis did not explicitly model the damage in the buffer strip. Even though the shear-lag model did not explicity model the damage, the shear-lag parameters were chosen to correlate with data from panels with damage. The shape of the curve is based on the mechanics in the model and is not a parameter. Only the data from the panels made with tape and from the uniweave panels with 12.7 mm wide buffer strips plies correlated well with the prediction. The data from

4 Mylar, registered trademark of E. I. duPont de Nemours and Co., Inc.

the uniweave panels with 6.4 mm and 3.2 mm buffer strips were below the predicted curve. Figure 11, as did figure 7, shows a substantially lower failing strain of panels with narrow buffer strip than panels with wide buffer strips.

The poor correlation for the data from panels with narrow buffer strips is due to the failure model assumed by the shear-lag model. The shear-lag model predicted panel failure when the first fiber in the buffer strip next to the crack failed. However, the panels with narrow buffer strips failed when the strain in the graphite fibers on the side of the buffer strip opposite the crack failed. Figure 12 shows strain data from a strip gage (13 strain gages spaced 2.03 mm on center) mounted over the buffer strip beyond the end of the slit. Strain is plotted versus distance from the center of the panel. Data shown are from just before the fracture initiated, just after arrest, and just before failure. The data taken just after arrest shows a sudden increase in strain in the buffer strip. The strains outside the buffer strip did not change much when the crack ran and arrested. The erratic strain readings in the region of the buffer strip are due to a delamination that formed between the outer 45° ply and the adjacent 0° ply. The delamination formed when the crack arrested. After the crack was arrested and the load was increased, the delamination continued to grow across the buffer strip until it reached the outer edge of the buffer strip. When the delamination reached the outer edge of the buffer strip the panel failed. Figure 12 shows that, just before failure, the strain just beyond the buffer strip was 0.01 which is the failing strain of a 0° graphite ply. It is likely that the panel failure began in the 0° plies of graphite just beyond the buffer strip and not in the buffer strip. The shear-lag model did not predict failure based on the graphite fiber but predicted failure based on the first fiber in the buffer strip adjacent to the crack. Without matrix damage, the strains in the buffer strip drop off sharply with distance from the crack and the failure of the panel will not begin in the graphite except for very narrow buffer strips. With damage, the stress concentration in the buffer strip is lowered, and it is

possible to fail the adjacent 0° graphite before failing the buffer material. For wide buffer strips, the damage did not grow across the buffer strip before overloading the S-glass fibers.

Shear Panels

Because fracture is controlled primarily by a tension stress field (mode I), a shear panel can be analyzed as a tension panel with an equal compressive stress applied transversely. For this reason, the slits in the shear panels were oriented perpendicular to the direction of the maximum tensile stress. The shear panels behaved like the tension buffer strip panels: the buffer strips arrested fractures that initiated from the slit and additional load was required to fail the panels. Figure 13 shows results from the $[0/45/90/-45]_{2S}$ shear panels; remote tensile strains are plotted against crack lengths. The curve represents the fracture analysis in [6] after superposition of the tensile and compressive stresses.

The analysis was developed using the principal of superposition; for an infinite sheet the shear stress on the panel was equivalent to the combined tension and compression stresses shown in Figure 14. Because the tensile and compressive stresses are uniaxial, the total strain in the y-direction in the shear panel is simply the sum of the y-direction strains in the tension and compression panels. Thus, the critical far-field longitudinal strain in the shear panel is

$$\varepsilon_y^* = \varepsilon_y{}^F + \varepsilon_y{}^P = \varepsilon_y{}^F + \frac{\nu_{yx}}{E_y}\ \tau_{x'y'}^* \tag{2}$$

where $\varepsilon_y{}^F$ is the critical far-field longitudinal strain in an infinite sheet loaded in uniaxial tension perpendicular to the crack, and $\varepsilon_y{}^P$ is the far-field longitudinal strain in an infinite sheet loaded in compression parallel to the crack. For specially orthotropic laminates with $E_x = E_y$, the critical shear stress is related to the longitudinal strain by transforming the extensional strains to the principal shear strain state and thus

$$\tau_{x'y'} = 2G_{x'y'}\ \varepsilon_y{}^* \tag{3}$$

where $G_{x'y'}$ is the effective shear modulus of the sheet in the x′y′ coordinate system (see fig. 4). Combining (2) and (3) and solving for $\tau^*_{x'y'}$ gives in terms of the fracture strain of the uniaxial sheet,

$$\tau^*_{x'y'} = \frac{2G_{x'y'}}{1 - \frac{2\nu_{yx} G_{x'y'}}{E_y}} \varepsilon_y{}^F \tag{4}$$

and substituting (4) into (2) gives

$$\varepsilon^*_y = \left[1 + \frac{2\nu_{yx}G_{x'y'}}{E_y - 2\nu_{yx}G_{x'y'}}\right]\varepsilon_y{}^F \tag{5}$$

where ν_{yx} and E_y are the effective Poisson's ratio and Young's modulus in the x,y coordinate system. For isotropic materials $\tau_{x'y'}$ and ε^*_y reduce to

$$\tau^*_{x'y'} = E\,\varepsilon_y{}^F \tag{6}$$

and

$$\varepsilon^*_y = (1 + \nu)\varepsilon_y{}^F \tag{7}$$

Finally using equation (4), where $\varepsilon_y{}^F$ is the predicted far-field failing strain of an infinite orthotropic sheet with a crack under uniaxial tensile load [6], the curve in figure 13 is obtained.

Figure 13 shows that the fracture initiation strains were below those predicted by the analysis. As mentioned previously, data from tests usually fall above or on the prediction. Data which coincides with the prediction ususally has little damage at the ends of the slit. Data which falls below the prediction indicates that the specimens are failing by a different mode or extrinsic loads. For these panels, the low fracture initiation stresses may be due to out-of-plane deformation (mode III) caused by the compressive stress parallel to the slit.

The shear panels were constrained from buckling and test results showed that the failing strain depended on the degree of constraint around the crack. The two panels with

the lowest failing strains (fig. 13) had constraint plates with cut-outs around the slit and adjacent buffer strips so that radiographs could be made under load. The panel with the highest failing strain had constraint plates with no cut-outs. Observation during testing suggested that once the crack had arrested, the damage grew, under additional load, as a local buckling failure in the unconstrained region and finally failed due to the compressive stress. Figure 15 shows a failed shear panel which was partially constrained. The compression failure started from the inside of the buffer strips adjacent to the slit, progressed parallel to the buffer strips in the unconstrained region, and at failure propagated under the constraint plates to the edge of the specimen. Failure of the fully constrained panels was similar except there was no stable growth of damage parallel to the buffer strips. The difference in the damage of fully constrained and partially constrained panels suggests that the fully constrained panels failed due to tensile fracture of the panel.

Figure 16 compares measured failing strain from the shear tests with predicted failing strain from the shear-lag model. The prediction was obtained by substituting the predicted failing strain of a tension panel (fig. 11) into equation (5). The shear-lag model, which accounted for damage in the buffer strip, overpredicted the failing strain of the fully constrained panels which suggests that there was less delamination and axial splitting in the shear panels than in the tension panels. Figure 17 shows radiographs of a tension and a shear buffer strip panel with arrested cracks. The radiographs were made near the failing strains of the panels. The radiograph of the tension panel shows that a delamination region has formed over the entire width of the buffer strip. As discussed earlier, such damage reduces the stress concentration in the 0° fibers and elevates strength. No such delamination region developed in the buffer strips of the shear panel. This indicates that the combined loading suppressed the delamination growth in the buffer strip, which of course reduced the strength.

The failing strain of the $[0/90]_{4S}$ panels were much lower than the failing strains of the $[0/45/90/-45]_{2S}$ panels. Reference 6 predicts that failing strains of all-graphite (0/90)

type laminates should be about two thirds that of (0/ ± 45/90) type laminates. The failing strains of buffer strip panels shown in figure 16 are in about the same proportion.

As mentioned previously, the shear panels were constrained to prevent buckling and thus to eliminate the influence of buckling or post-buckling on the fracture results. However; in design, panel buckling must be addressed. For the quasi-isotropic panels tested in shear, the critical elastic buckling stress was determined from [9]

$$\tau_{x'y'}^{B} = \frac{64\pi^2 K_s h_o^{\,2}}{3L_s(1-\nu^2)} \tag{8}$$

where $K_S = 15$ and is the boundary condition correction factor and $L_S = 305$ mm and is the length of a side of the panel. Using equations (6) and (8), figure 18 shows the ratio of $\tau_x^{*}{}'_{y'}$ to $\tau_x^{B}{}'_{y'}$ versus panel thickness for plain panels with various slit lengths and for a panel with 12.7 mm wide buffer strips and an arrested crack. The figure shows that for panels with realistic thicknesses (48 plies is 7 mm) shear panels may be fracture critical. For larger slits or damage, panels are more likely to fail due to fracture. In contrast, a buffer strip panel is more likely to fail due to buckling because the buffer strips elevate the fracture stress. It must be emphasized that an elastic buckling analysis was used to obtain figure 18 and the post-buckling behavior has not been taken into account. Post-buckling will alter the results shown in the figure because the post-buckled panel strength is greater than the elastic buckling stess.

CONCLUSIONS

The fracture behavior of buffer strip panels was studied. The panels were made with a uniweave graphite cloth, where the S-glass buffer strips were woven into the cloth. Panels were tested in tension and shear. Specimens were loaded at a constant rate while far-field strain, strain in the buffer strips, and COD were measured. From the tests and a shear-lag model for buffer strip panels, it was concluded that

1. Tension buffer strip panels made from uniweave graphite cloth had about the same failing strain as panels made from prepreg tape. The buffer strips arrested the cracks, and the failing strain (or strength) was much higher than the failing strain of all-graphite panels with similar damage.
2. Buffer strip panels tested in shear arrested cracks like panels tested in tension.
3. Buffer strip geometry significantly affected the failing strain of panels with arrested cracks. Panel strengths increase with both buffer strip width and buffer strip thickness. For panels with narrow buffer strips, strain measurements showed the panels failed when the strain in the graphite just beyond the buffer strip reached the failing strain of 0° graphite. Panels with wide buffer strips failed when the buffer strips failed.
4. Panels with buffer material in every ply had the highest strength and were notch insensitive (net section stress equals the tensile ultimate strength).
5. The shear-lag model predicted the failing strain of tension panels with wide buffer strips accurately. The model overestimated the failing strain of tension panels with narrow buffer strips because the failure mode in the panels was different than the failure criterion used in the model. The model overestimated the failing strain of the shear panels also. The discrepancy was attributed to the size of the damage region in the buffer strips.

REFERENCES

1. Poe, C.C., Jr. and Kennedy, John M.: "An Assessment of Buffer Strips for Improving Damage Tolerance of Composite Laminates," Journal of Composite Materials Supplement, Vol. 14, 1980, pp. 57-70.
2. Kennedy, John M.: "Fracture Behavior of Hybrid Composite Laminates," Proceedings of the 24th AIAA/ASME/ASCE/AHS Structures, Structure Dynamics, and

Materials Conference, Lake Tahoe, NV, May 1983, AIAA Paper No. 83-0804, pp. 68-78.

3. Goree, James G. and Kaw, Autar K.: "Shear-Lag Analysis of Notched Laminates with Interlaminar Debonding," NASA CR-3798, 1984.

4. Bonnar, G.R. and Palmer, R.J.: "Woven Graphite Epoxy Composite Test Specimens with Glass Buffer Strips," NASA CR-165871, 1982.

5. Farley, Gary L. and Baker, Donald J.: "In-plane Shear Test of Thin Panels," Experimental Mechanics, Vol. 23, No. 1, March 1983, pp. 51-57.

6. Poe, C.C., Jr.: "A Unifying Strain Criterion for Fracture of Fibrous Composite Laminates," Engineering Fracture Mechanics, Vol. 17, No. 2, 1983, pp. 153-171.

7. Poe, C.C., Jr.: "Fracture Toughness of Fibrous Composite Materials," NASA TP-2370, 1984.

8. Harris, C.E. and Morris, D.H.: "Fracture Behavior of Thick, Laminated Graphite/Epoxy Composites," NASA CR-3784, 1984.

9. Brush, Don O. and Almorth, Bo O.: Buckling of Bars, Plates, and Shells, McGraw-Hill Book Company, New York, 1975.

APPENDIX

The analysis in [6] was developed to predict the notched strength for any laminate orientation. The panels tested herein were 0° ply dominated, and thus the analysis simplified considerably. From [6], the strains at the crack-tip in mode I loading for a 0° ply are

$$\begin{Bmatrix} \varepsilon_1 \\ \varepsilon_2 \\ \gamma_{12} \end{Bmatrix} = \frac{K_\varepsilon}{\sqrt{2\pi r}} \begin{Bmatrix} 1 - \nu_{yx}\sqrt{\frac{E_y}{E_x}} \\ \sqrt{\frac{E_y}{E_x}} - \nu_{yx} \\ 0 \end{Bmatrix} \tag{A1}$$

Assuming that the laminate fails when the axial strain parallel to the fibers in the principle load carrying laminae becomes critical, then $\varepsilon_1\sqrt{2\pi r}$ will be a constant at failure which leads to

$$\varepsilon_1\sqrt{2\pi r} = K\varepsilon_Q(1-\nu_{yx})\sqrt{\frac{E_x}{E_y}} = Q_c \qquad \text{(A2)}$$

where Q_c is defined as a general fracture toughness parameter. Poe [6] showed that for a large class of laminates

$$Q_c = 1.5\,\varepsilon_{tuf} \qquad \text{(A3)}$$

Thus, using A2 and A3 fracture strains of laminates under uniaxial loading can be predicted from

$$\varepsilon_y{}^F = \frac{K\varepsilon_Q}{\sqrt{\pi(a+\delta_c)}} \qquad \text{(A4)}$$

Table 1. Specifications of Buffer Strip Panels and Test Results

Laminate (x,y cord.)	Test Type	W_b, mm	h_b, mm	Buffer Plies	Panel No.	Slit Length, mm	Fracture Initiation Strain, ε_y	Failure Strain, ε_y^F	Panel[C] Modulus, GPa
$[45/0/-45/90]_{2s}$	Tension	12.7	0.15	0°	1	12.7	.004654	.005884	47.35
					2	25.4	.003530	.005877	45.99
					3	25.4	.003710	.006114	46.41
					4	44.5	.003167	.006128	45.44
		6.4	0.15	0°	1	12.7	.003770	.00377[a]	52.63
					2	38.1	.001965	.004101	53.97
					3	44.5	.002466	.004215	48.78
		6.4	0.30	0°	1	12.7	.004398	.005661	45.84
					2	25.4	.003436	.005691	45.35
					3	44.5	.002829	.005522	48.08
		3.2	0.15	0°	1	25.4	.003269	.003269[a]	42.52
					2	38.1	.002458	.003549	45.19
					3	44.5	.002379	.003583	47.64
		3.2	0.61	0°	1	12.7	.004405	.004405[a]	44.06
					2	25.4	.003300	.004853	46.39
					3	44.5	.002913	.004817	45.95
		12.7	0.15	0°,+45°,90	1	5.1	.008007	.008007[a]	43.39
					2	12.7	.006703	.008000	43.86
					3	25.4	.005209	.008001	43.47
$[45/0/-45/90]_{6s}$	Tension	12.7	0.15	0°	1	12.7	.004121	.005519	45.50
					2	25.4	.003338	.005619	48.41
					3	44.5	.002371	.005500	49.22
$[0/90]_{4s}$	Shear	12.7	0.15	0°,90°	1	12.7	.002585	.002601	24.60
					2	25.4	.002074	.002536	23.87
					3[b]	25.4	.001855	.003113	24.53

Table 1. Concluded

Laminate (x,y cord.)	Test Type	W_b, mm	h_b, mm	Buffer Plies	Panel No.	Slit Length, mm	Fracture Initiation Strain, ε_y	Failure Strain, ε_y^F	Panel[C] Modulus, GPa
					4	44.5	.001606	.002554	33.03
					1	12.7	.004801	.004814	15.56
$[0/45/90/-45]_{2s}$	Shear	12.7	0. 15	0°,90°	2	25.4	.003707	.004986	14.96
					3[b]	25.4	.003947	.006195	13.97

[a] Fracture did not arrest, panel failed when fracture initiated

[b] Fully constrained from buckling

[c] Value given is extensional modulus for tension panels and shear modulus for shear panels.

Table 2. Results of Unnotched and Notched Tensile Tests

a. Unnotched

Laminate	E_y, GPa	E_x, GPa	ν_{xy}	ν_{xy}	S_{cy}, MPa	S_{cx}, MPa	$\varepsilon_y{}^F$	$\varepsilon_x{}^F$
$[45/0/-45/90]_{2s}$	48.59	48.50	.3130	.3063	435.4	450.1	.00918	.00925
$[45/0_{G1}/-45/90]_{2s}$	27.94	44.22	.3086	.4808	350.2	427.9	.02227	.00993

b. Notched

Laminate	2a, mm	W, mm	S_{cy}, MPa	$\varepsilon_y{}^F$	K_{EQ}, $\sqrt{mm}$
$[45/0/-45/90]_{2s}$	8.5	50.8	218.3	.00444	.0189
	16.9	50.8	147.7	.00327	.0196
	25.4	50.8	110.1	.00210	.0164
	33.8	101.6	122.9	.00226	.0185
	50.8	101.6	78.2	.00163	.0177
$[45/0_{G1}/90]_{2s}$	8.5	50.8	282.8	.01133	.0491
	16.9	50.8	212.9	.00810	.0488
	16.9	50.8	199.1	.00796	.0478
	16.9	101.6	269.1	.01093	.0662
	25.4	50.8	160.8	.00569	.0448
	34.3	101.6	201.9	.00791	.0677
	55.9	101.6	133.1	.00486	.0587

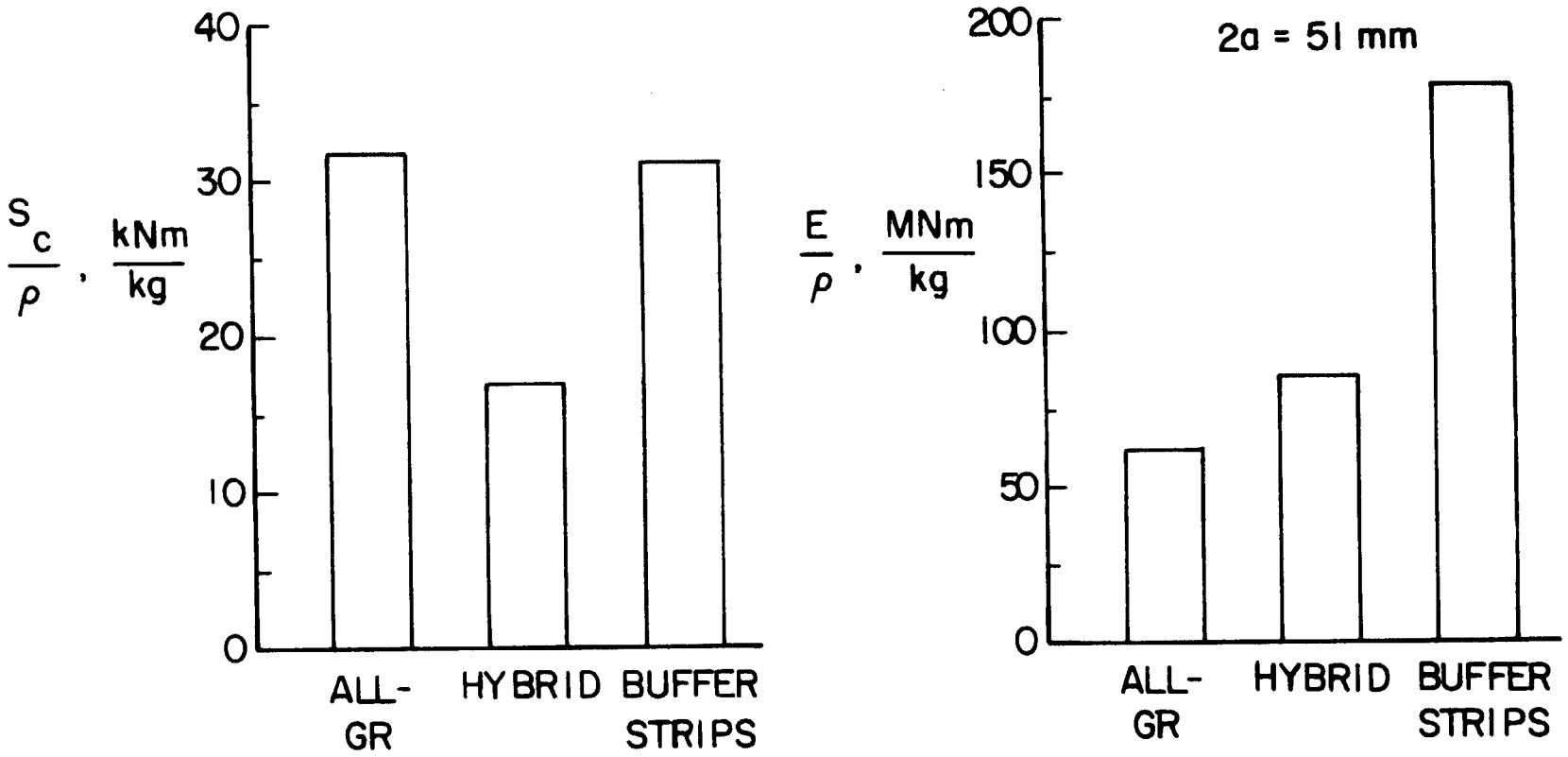

a) specific modulus

b) specific strength

Figure 1. Specific modulus and strength of composite panels

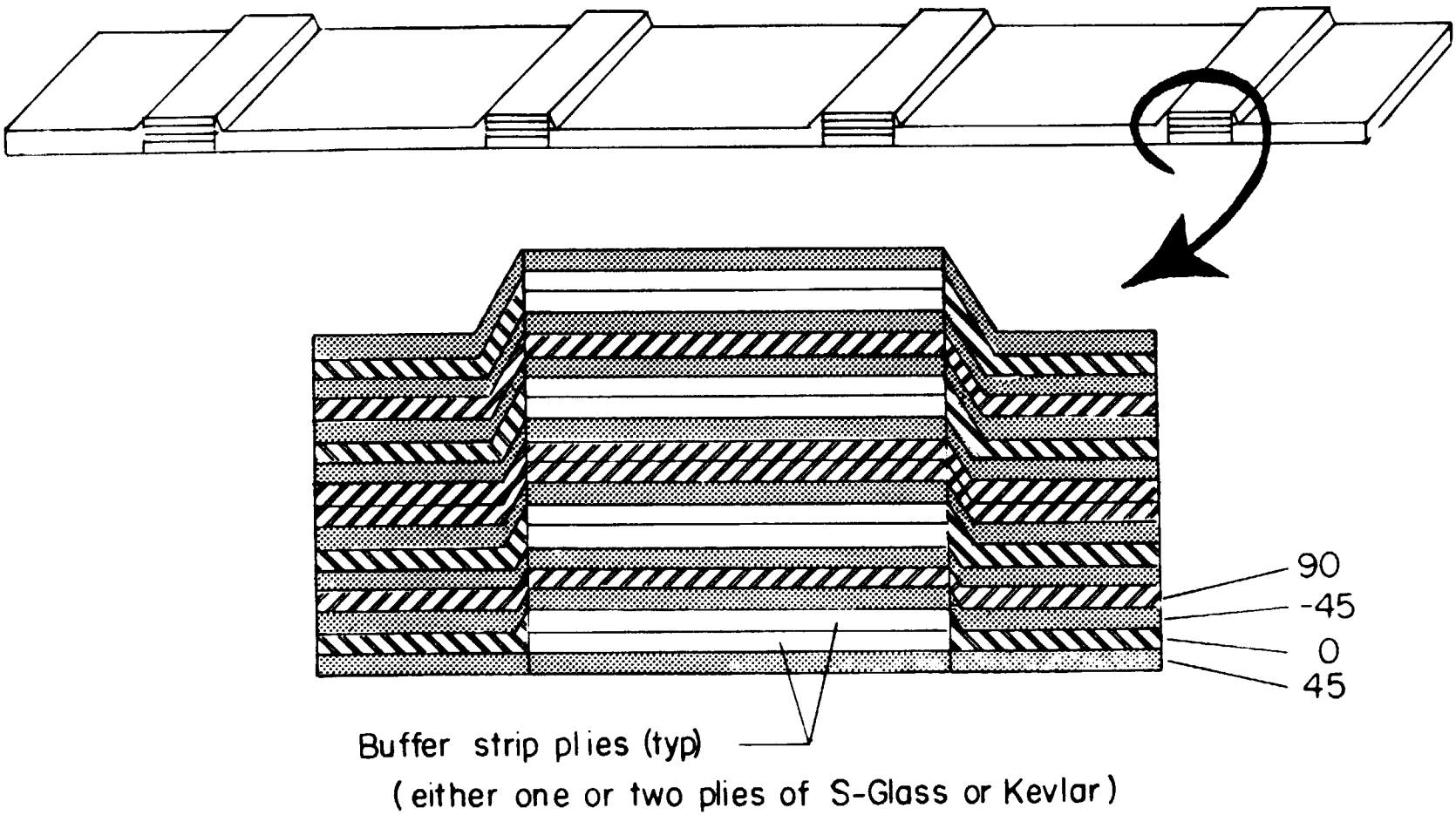

Figure 2. Cross-section of a typical buffer strip panel.

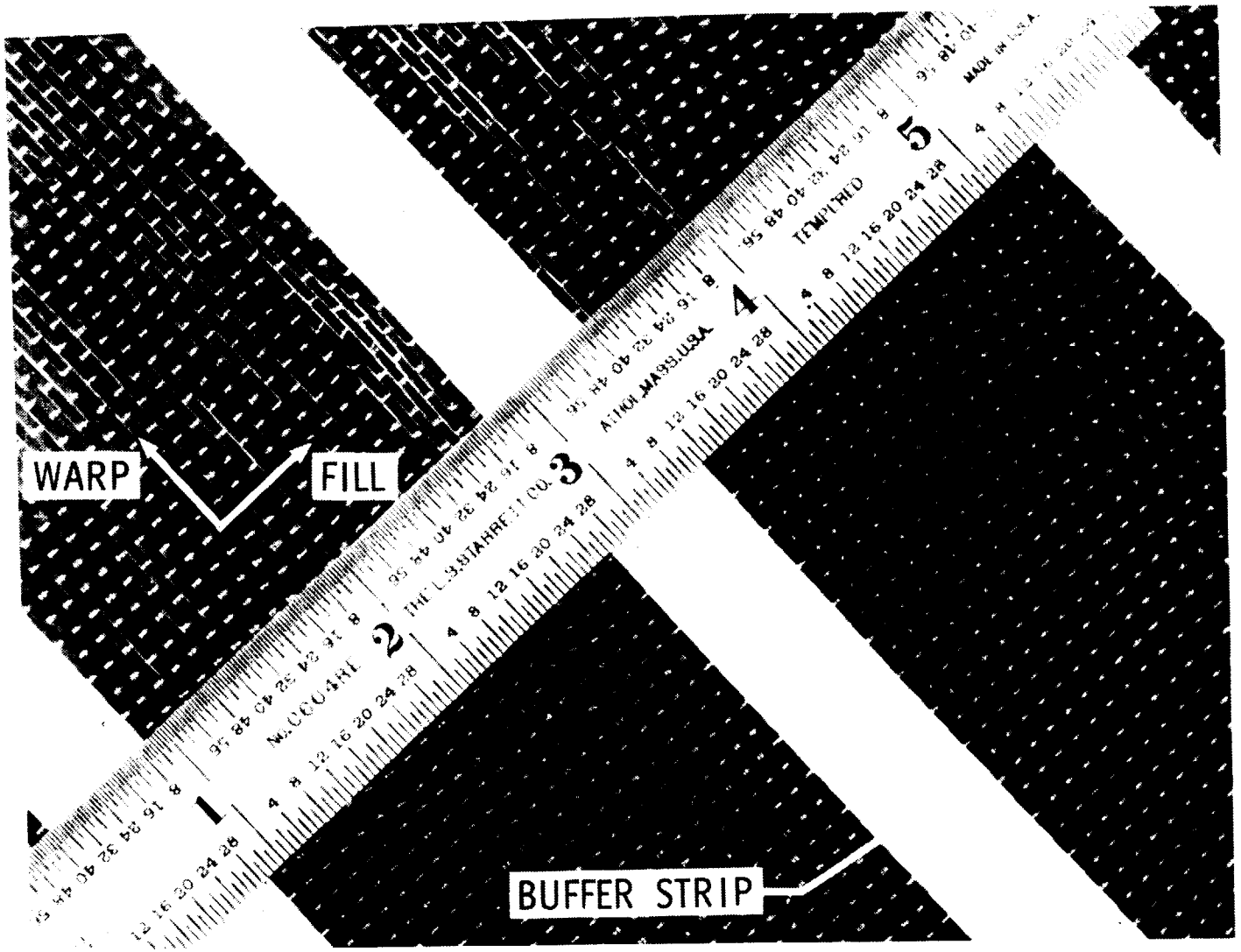

Figure 3. Uniweave cloth with 12.7 mm wide buffer strips.

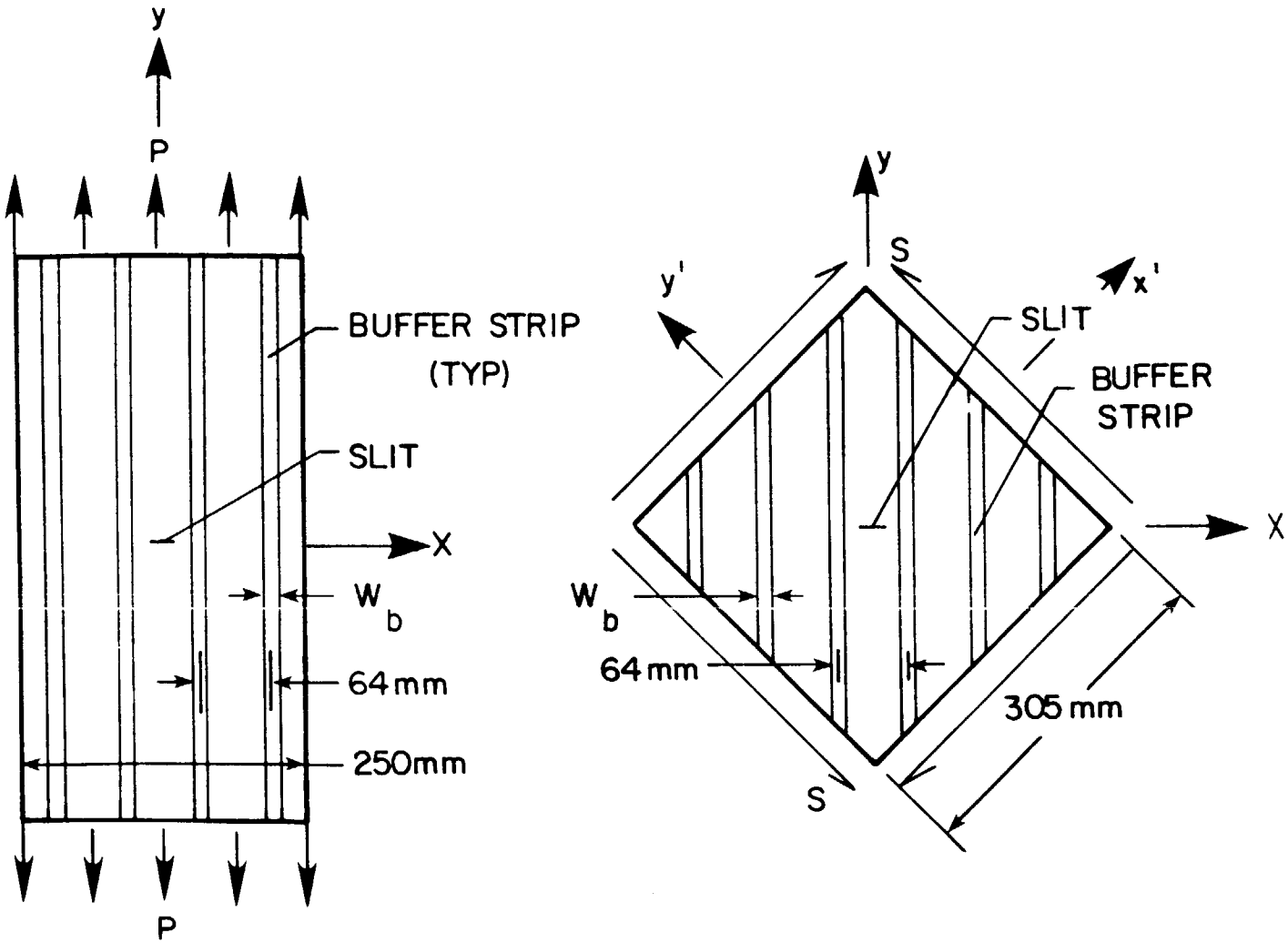

a) tension

b) shear

Figure 4. Test panel configurations

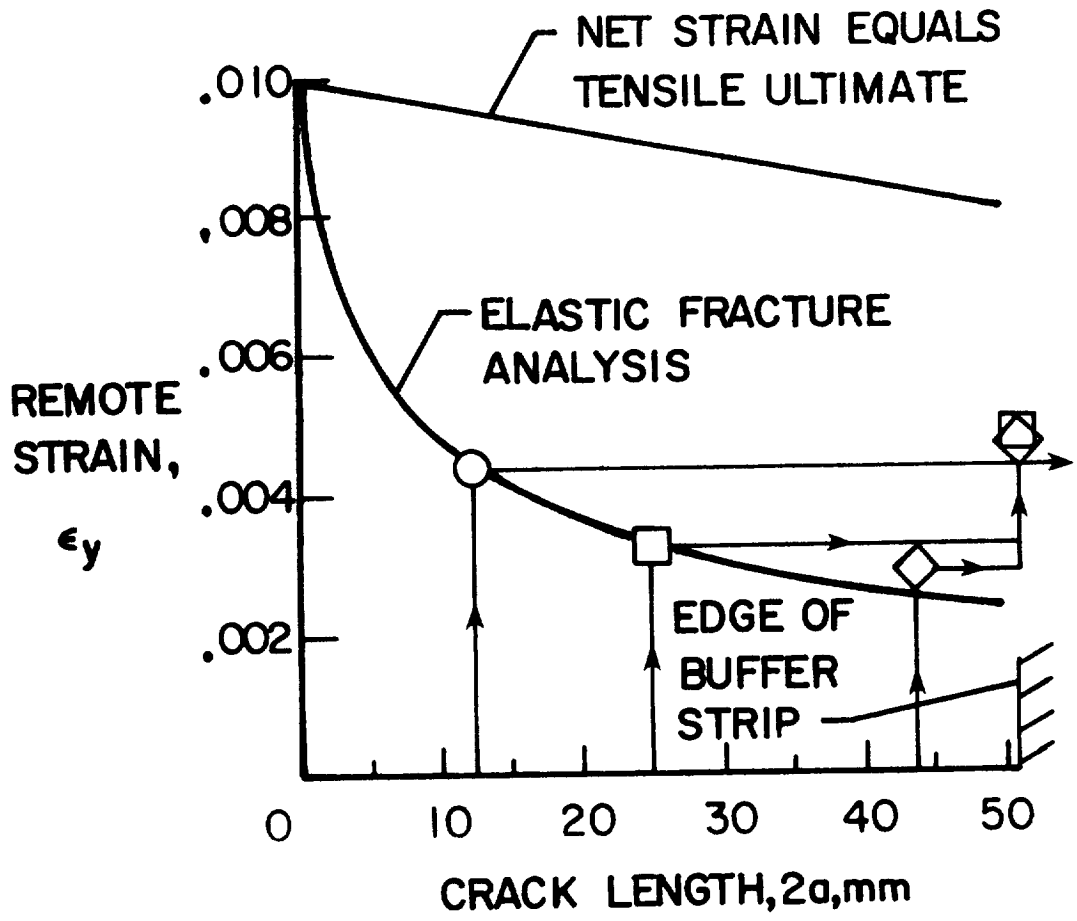

Figure 5. Fracture arrest results for tension buffer strip panels with 3.2 mm wide and 0.61 mm thick buffer strips.

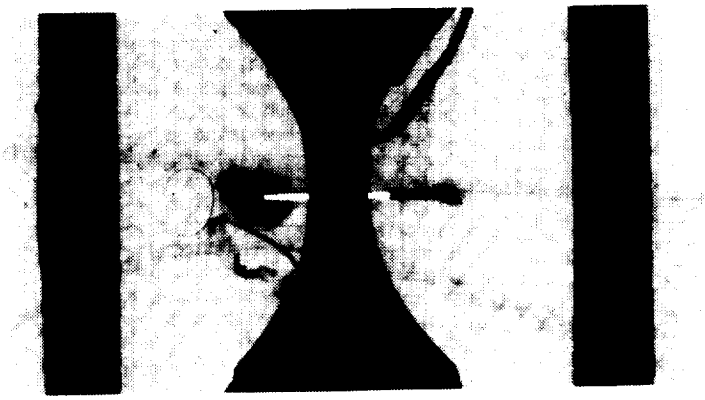

a) before initiation

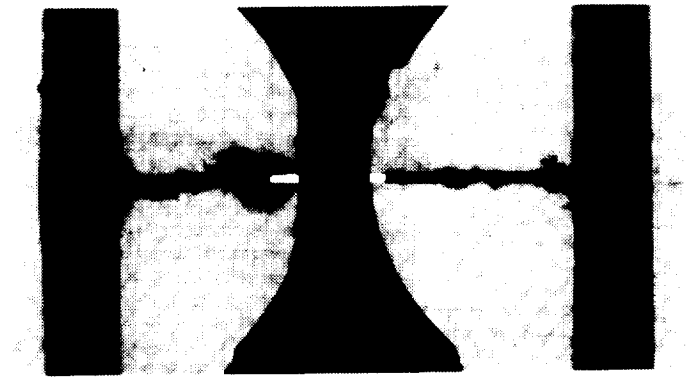

b) after arrest

Figure 6. Radiographs of a tension buffer strip panel with 3.2 mm wide and 0.61 mm thick buffer strips.

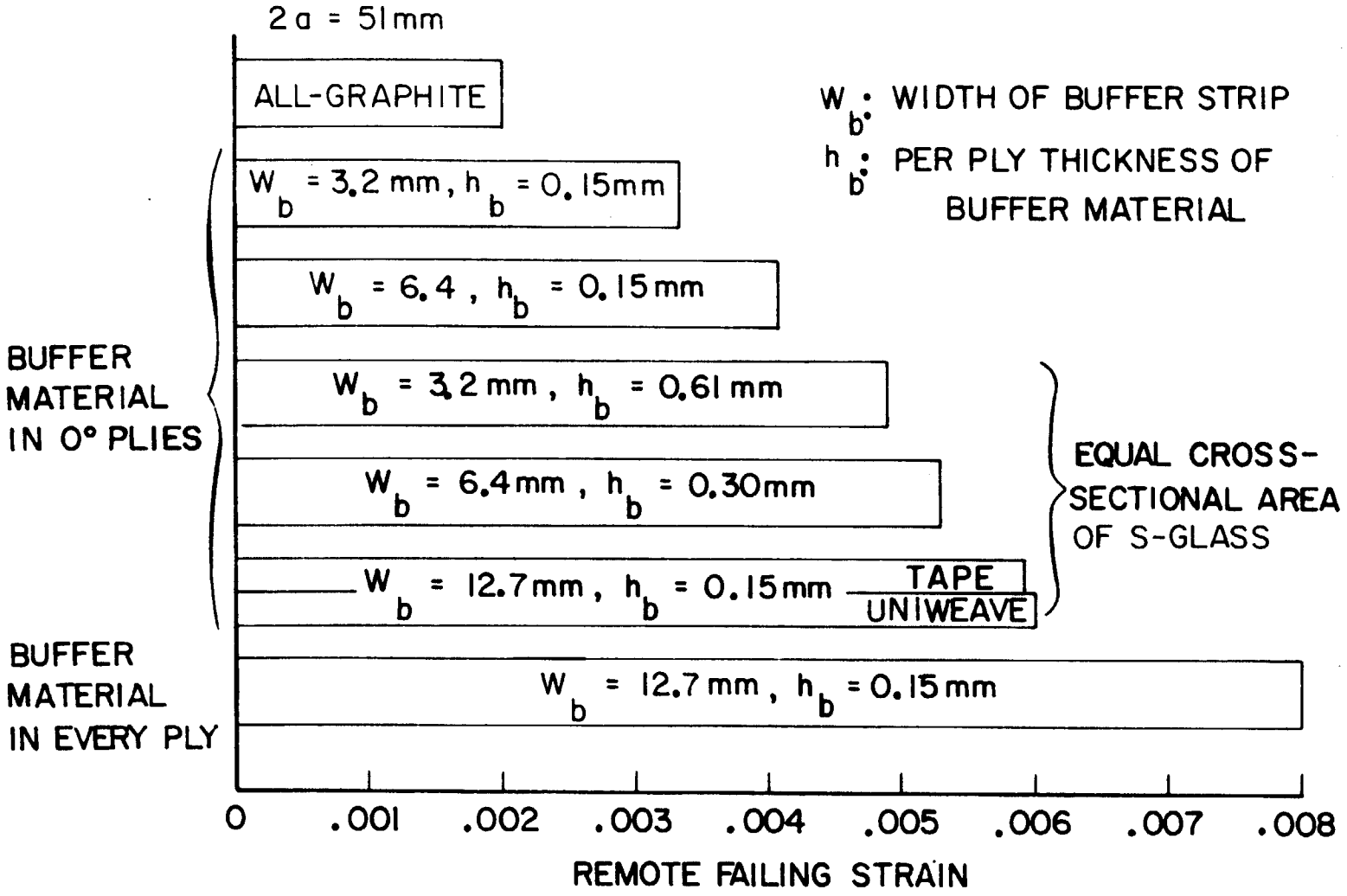

Figure 7. Remote failing strain of tension buffer strip panels with arrested cracks.

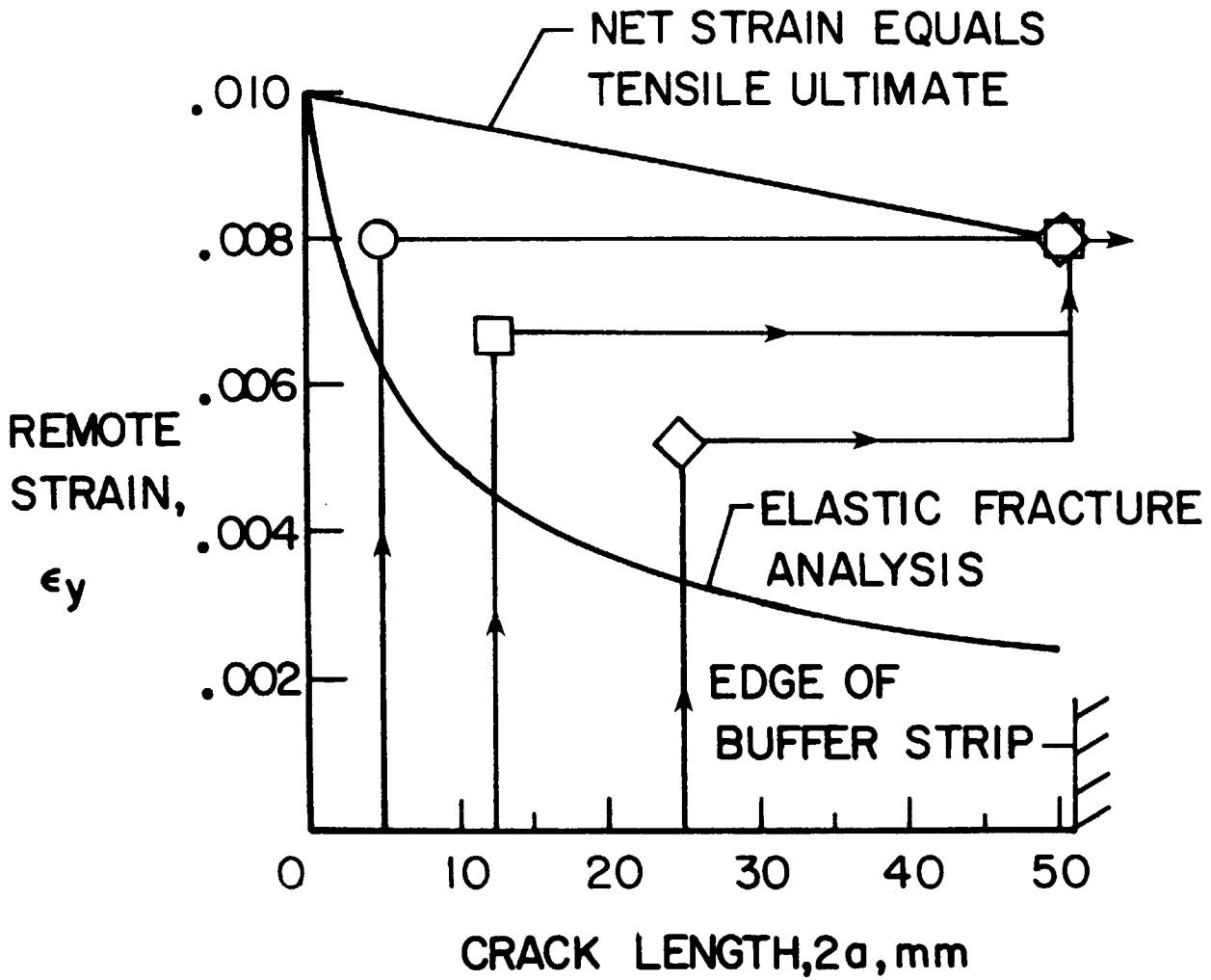

Figure 8. Fracture arrest results for tension buffer strip panels with 12.7 mm buffer strips in every ply.

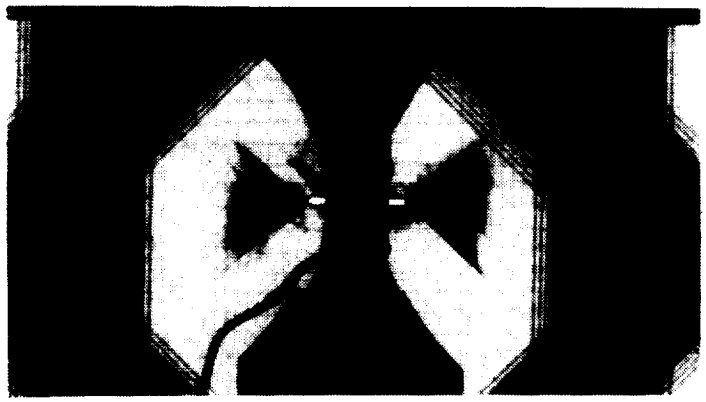

a) before arrest

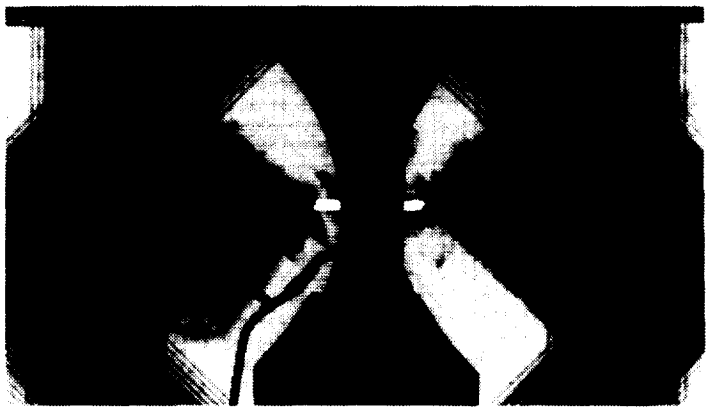

b) after arrest

Figure 9. Radiographs of a tension buffer strip panel with buffer strips in every ply.

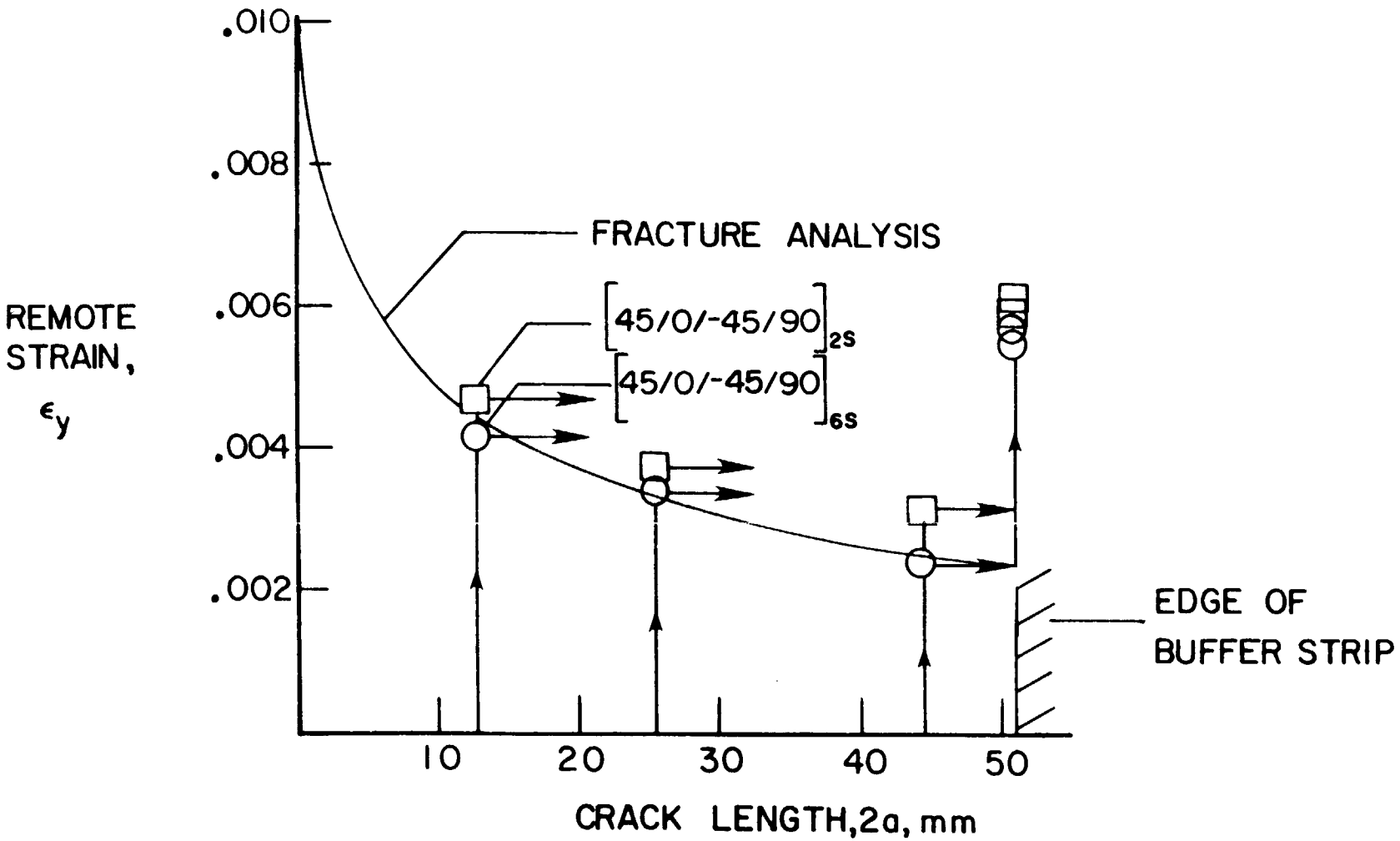

Figure 10. Fracture data from $[45/0/-45/90]_{6s}$ buffer strip panels, W_b = 12.7 mm.

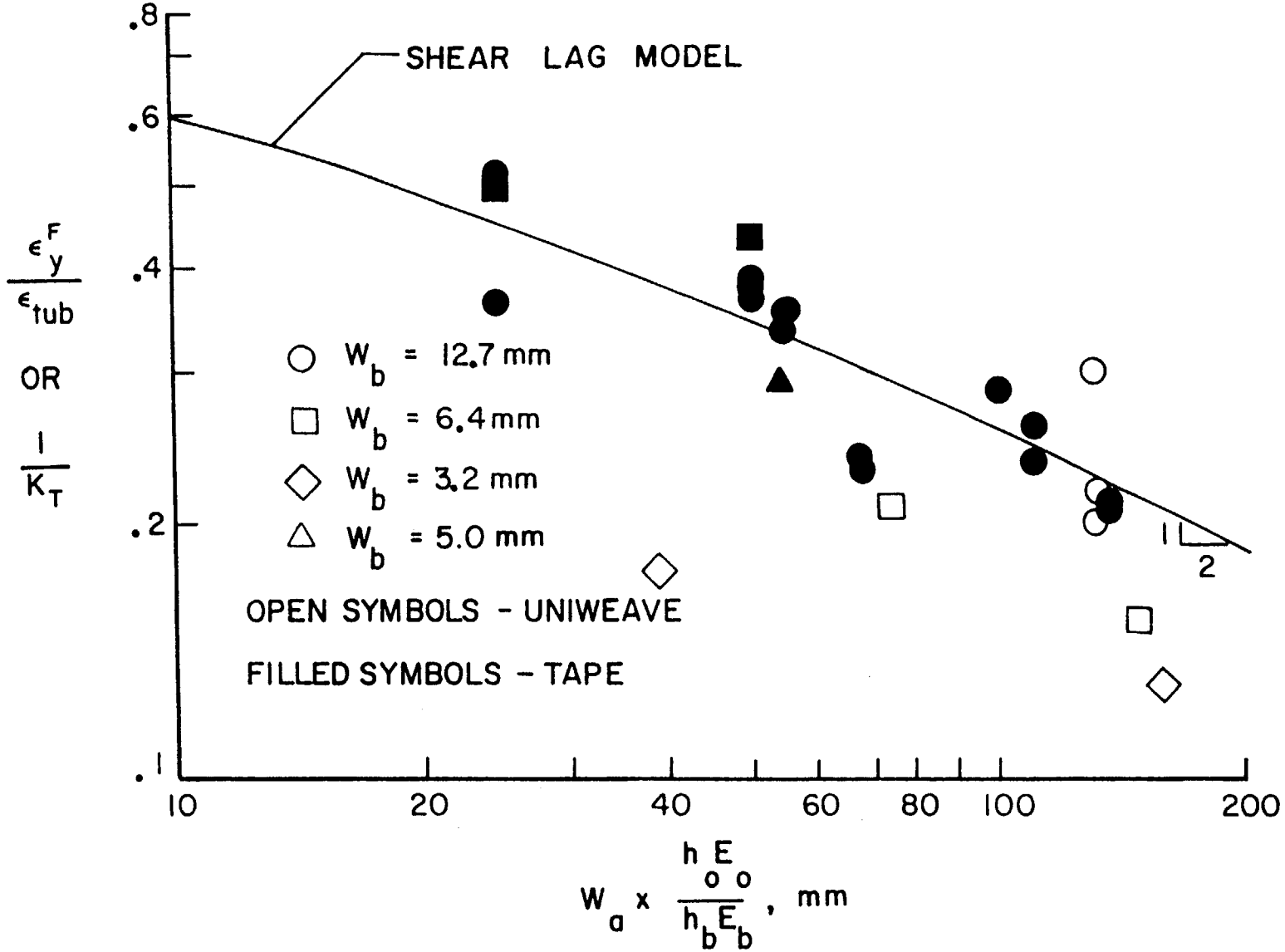

Figure 11. Correlation of experimental and analytical results for buffer strip panels with arrested cracks.

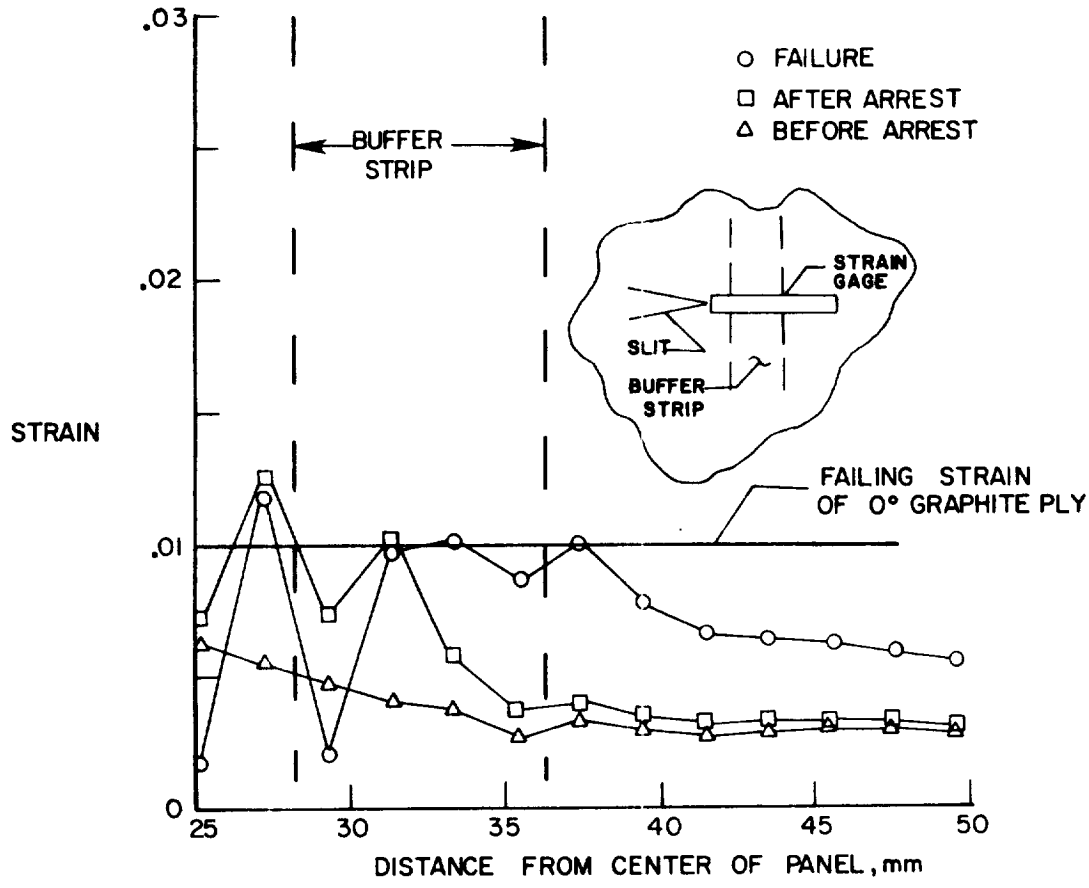

Figure 12. Local strain in the buffer strip along the line of the crack, W_b = 6.4 mm.

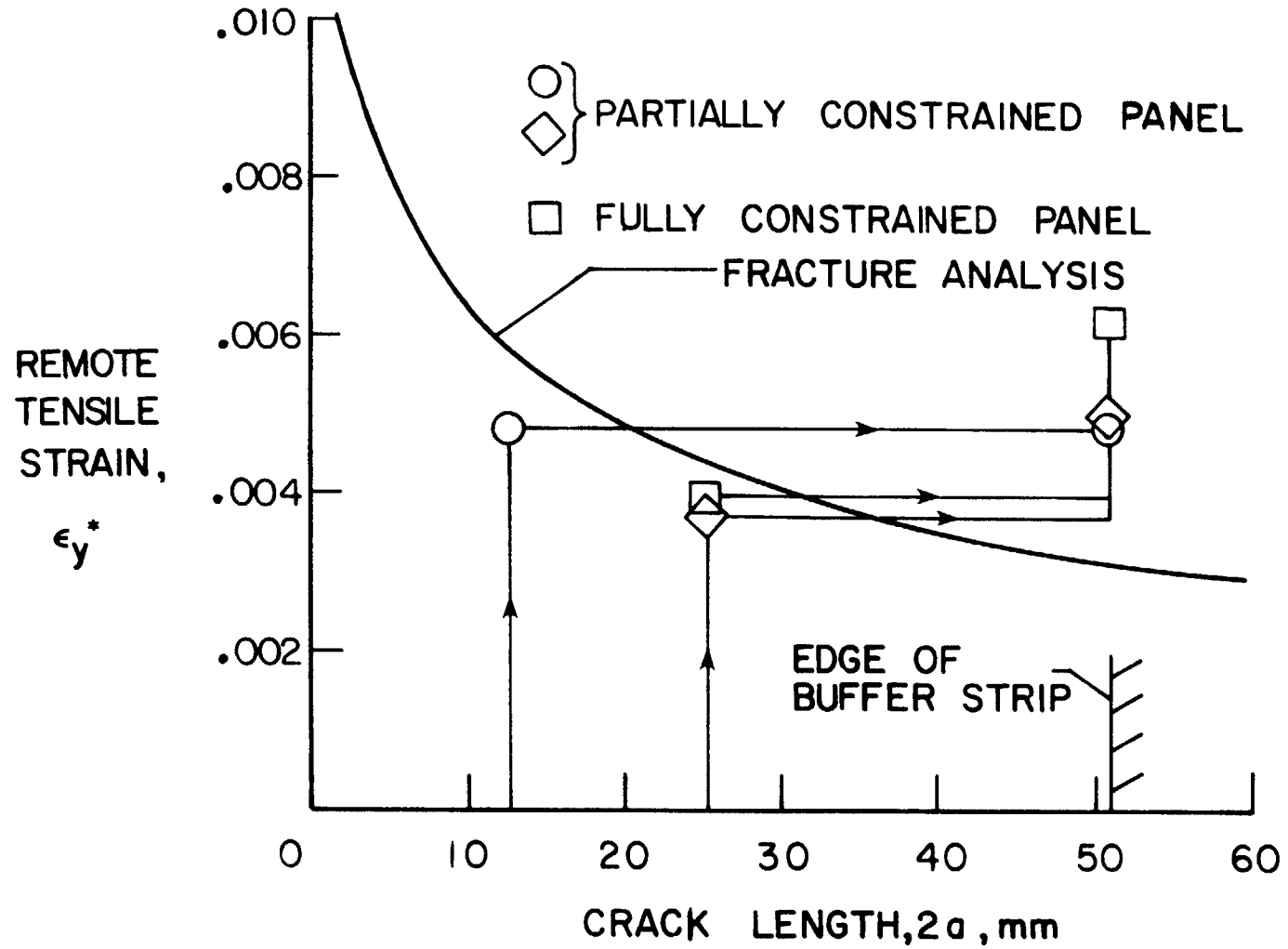

Figure 13. Remote tensile strain verses crack length for $[0/45/90/-45]_{2s}$ shear buffer strip panel, $W_b = 12.7$ mm.

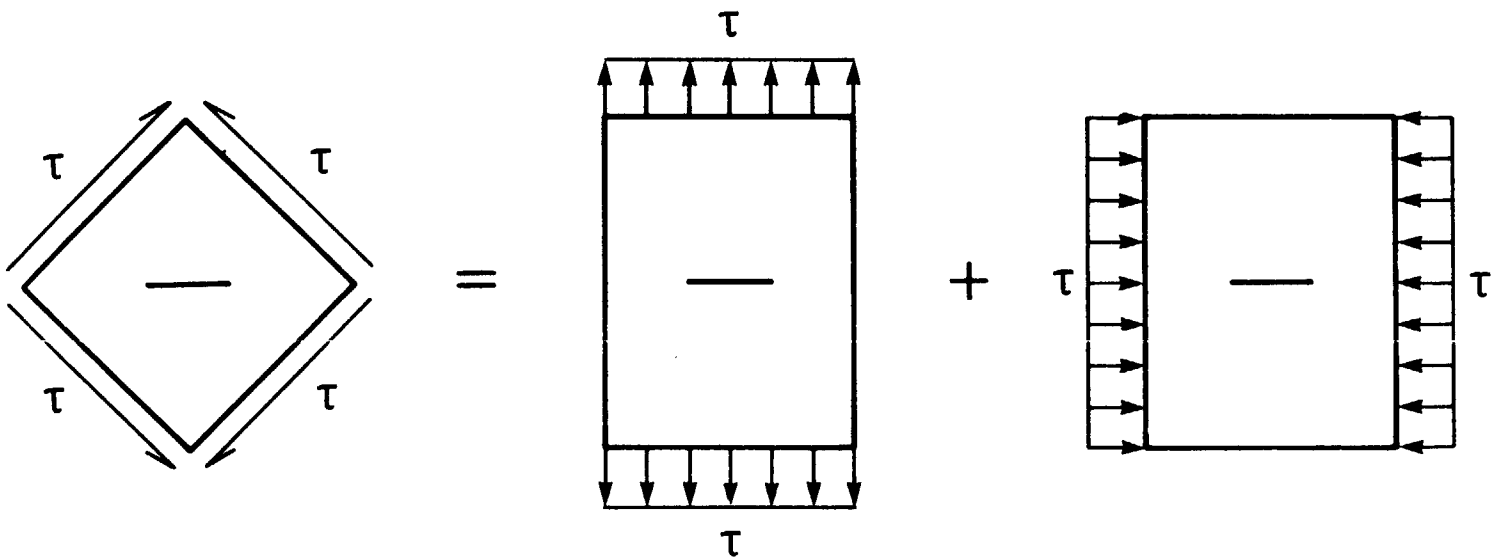

Figure 14. Far-field shear stress due to superposition of far-field axial stresses.

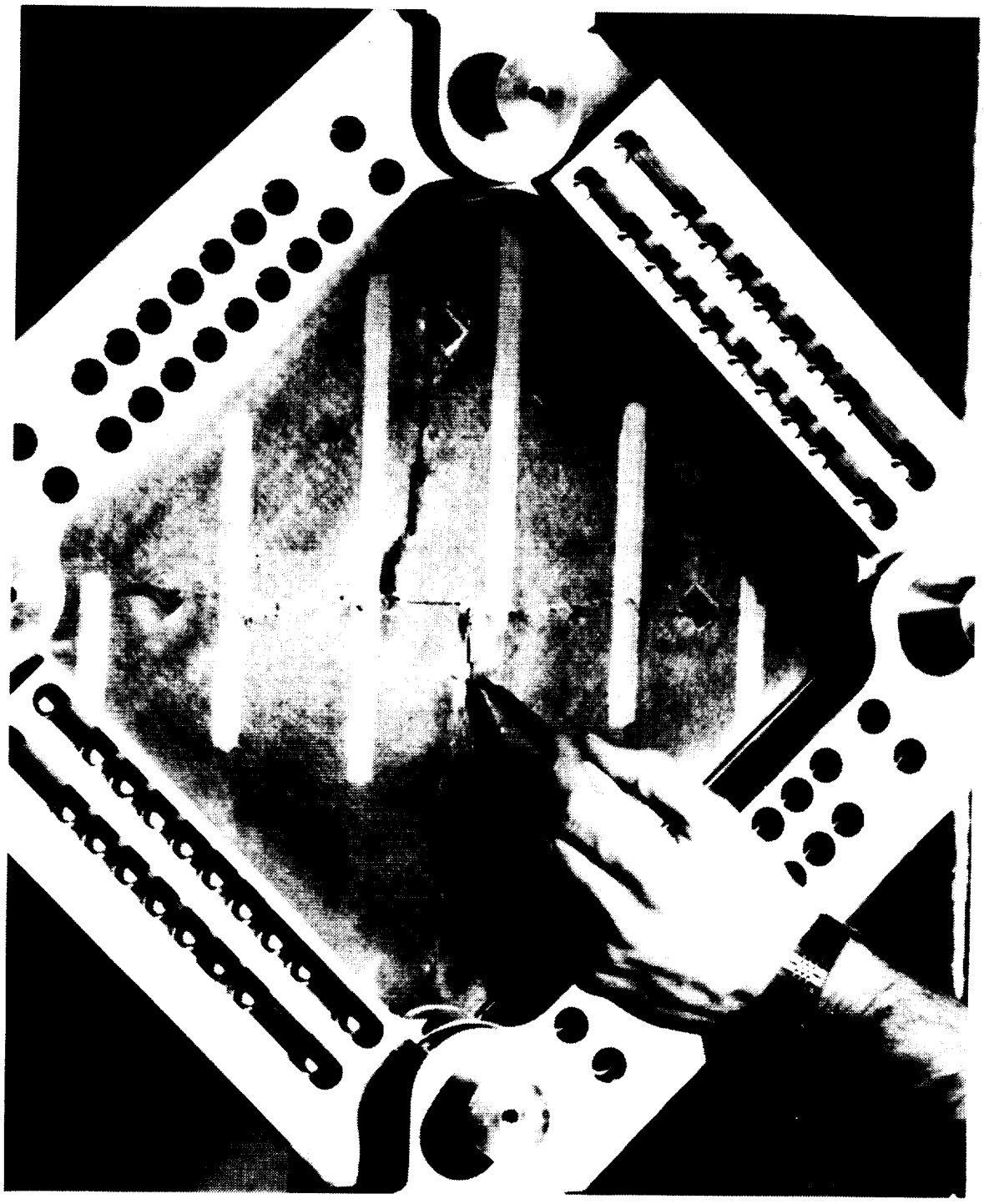

Figure 15. Failed $[0/45/90\text{-}45]_{2s}$ buffer strip panel after testing under shear load.

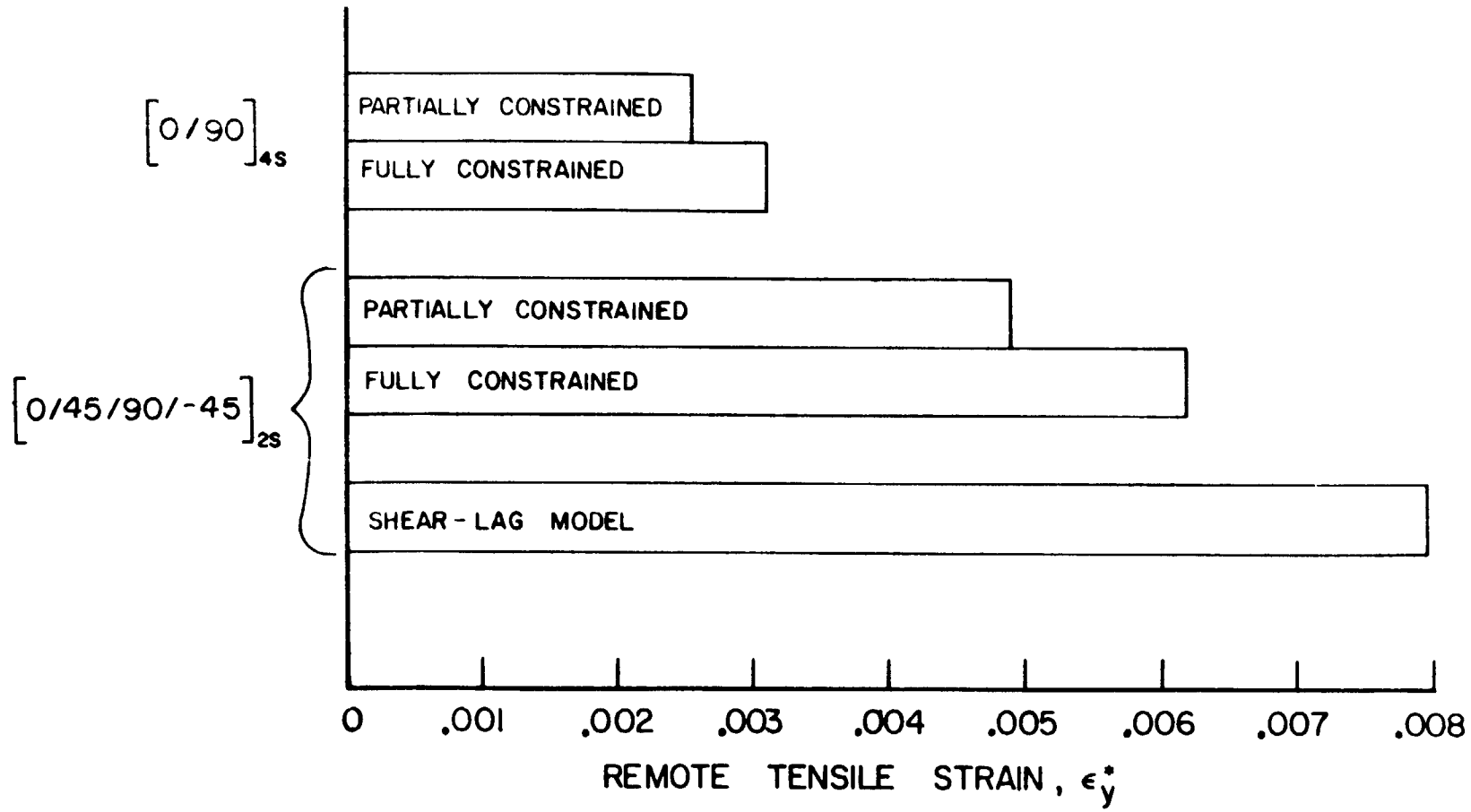

Figure 16. Predicted and measured failing strain of buffer strip panels tested in shear.

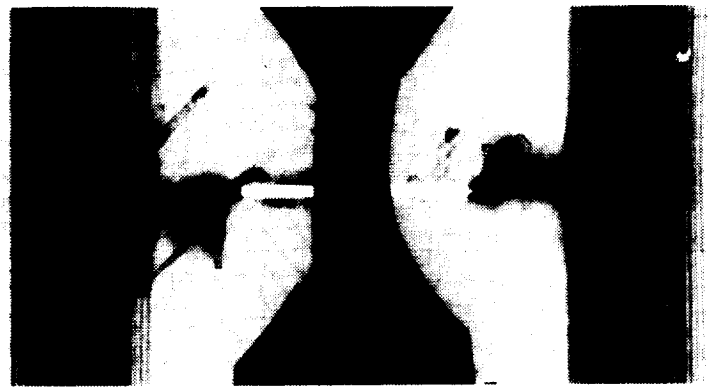

a) Tension, $\varepsilon_y = 0.99591$

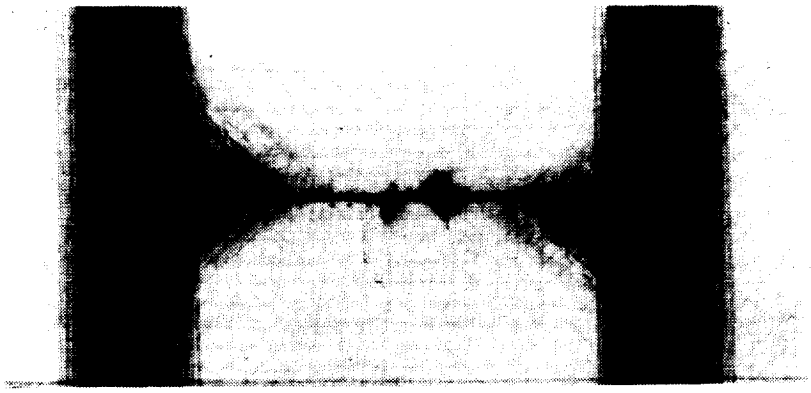

b) Shear, $\varepsilon_y = 0.00634$

Figure 17. Radiographs of [45/0/-45/90]2s tension and $[0/45/90/-45]_{2s}$ shear buffer strrip panels, $W_b = 12.7$ mm.

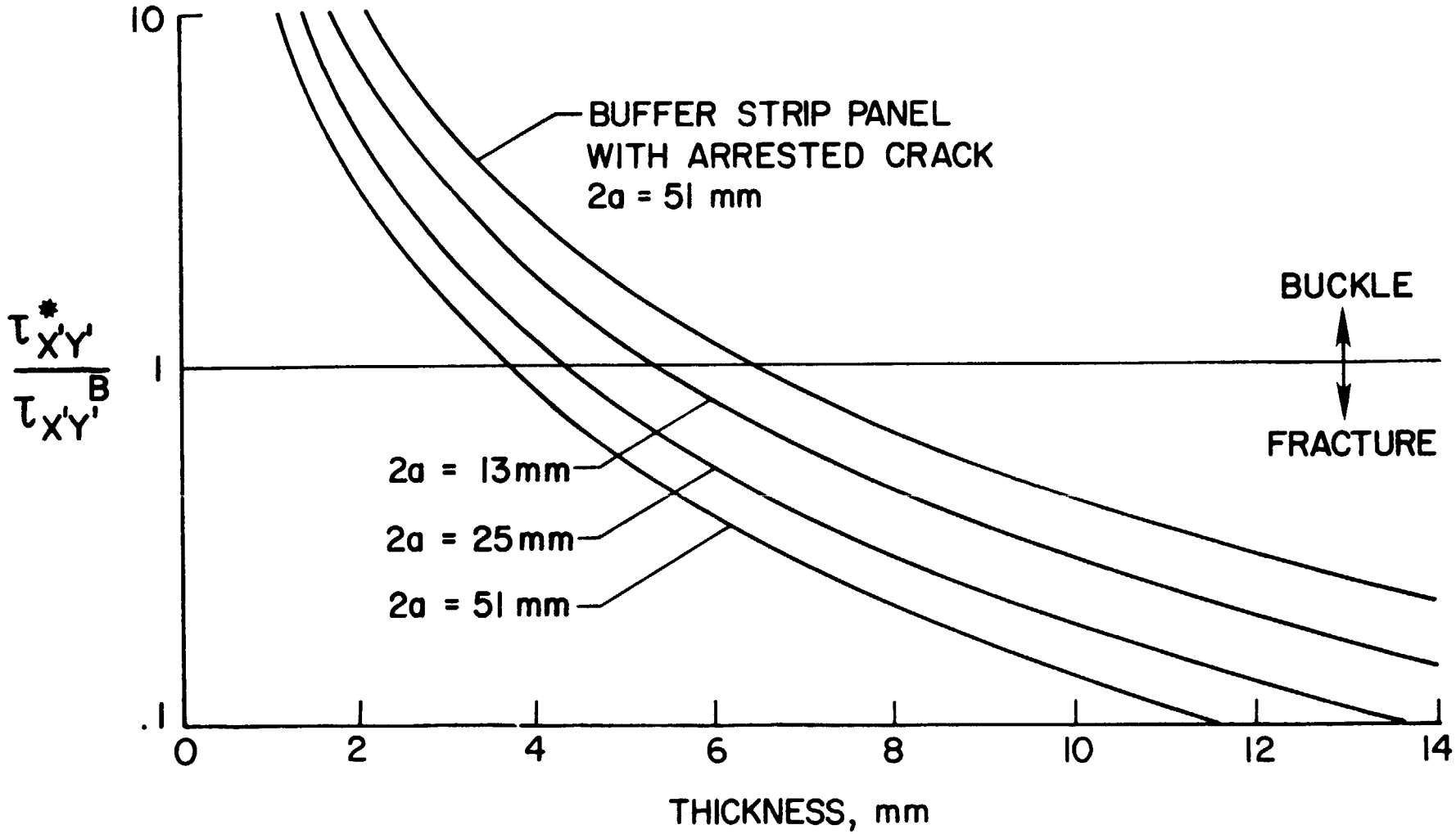

Figure 18. Comparison of fracture strength to buckling stress for quasi-isotropic shear panels with slits.

NASA
National Aeronautics and Space Administration

Report Documentation Page

1. Report No.	2. Government Accession No.	3. Recipient's Catalog No.
NASA TM-102702		

4. Title and Subtitle

Damage Tolerance of Woven Graphite/Epoxy Buffer Strip Panels

5. Report Date

August 1990

6. Performing Organization Code

7. Author(s)

John M. Kennedy

8. Performing Organization Report No.

10. Work Unit No.

505-63-01-05

9. Performing Organization Name and Address

NASA Langley Research Center
Hampton, VA 23665-5225

11. Contract or Grant No.

13. Type of Report and Period Covered

Technical Memorandum

12. Sponsoring Agency Name and Address

National Aeronautics and Space Administration
Washington, DC 20546-0001

14. Sponsoring Agency Code

15. Supplementary Notes

Dr. John M. Kennedy, Department of Mechanical Engineering and Engineering Mechanics, Clemson University, Clemson, SC 29631. Dr. Kennedy was employed by NASA when report was written.

16. Abstract

Graphite/epoxy panels with S-glass buffer strips were tested in tension and shear to measure their residual strengths with crack-like damage. The buffer strips were regularly spaced narrow strips of continuous S-glass. Panels were made with a uniweave graphite cloth where the S-glass buffer material was woven directly into the cloth. Panels were made with different width and thickness buffer strips. The panels were loaded to failure while remote strain, strain at the end of the slit, and crack opening displacement were monitored. The notched region and nearby buffer strips were radiographed periodically to reveal crack growth and damage.

Except for panels with short slits, the buffer strips arrested the propagating crack. The strength (or failing strain) of the panels was significantly higher than the strength of all-graphite panels with the same length slit. Panels with wide, thick buffer strips were stronger than panels with thin, narrow buffer strips. A shear-lag model predict the failing strength of tension panels with wide buffer strips accurately, but over-estimated the strength of the shear panels and the tension panels with narrow buffer strips.

17. Key Words (Suggested by Author(s))	18. Distribution Statement
Composites Damage tolerance Fracture Buffer strips Tension Shear	Unclassified - Unlimited Subject Category - 39

19. Security Classif. (of this report)	20. Security Classif. (of this page)	21. No. of pages	22. Price
Unclassified	Unclassified	41	A03